Optimization Of Water Droplet Impact On GFRP Blade Materials With Taguchi Technique

Amanpreet Singh[1], Mohit Yadav[2*], Osamah Ibrahim Khalaf[3*], Mohammed Sahib Mahdi Altaei[4], Khushwant Singh[5], and Fernando Moreira[6,7]

[1] *Department of Mechanical Engineering, Chandigarh University, Mohali-140413, Punjab, India*
[2] *Department of Mathematics, University Institute of Sciences, Chandigarh University, Mohali-140413, Punjab, India*
[3] *Department of Solar, Al-Nahrain Renewable Energy Research Center, Al-Nahrain University, Jadriya, Baghdad, Iraq*
[4] *Department of Computer Science, College of Science, Al-Nahrain University, Baghdad, Iraq*
[5] *University School of Information, Communication & Technology, Guru Gobind Singh Indraprastha University, New Delhi-110075, India*
[6] *Research on Economics, Management, and Information Technologies (REMIT), Universidade Portucalense, 4200-072, Porto, Portugal*
[7] *IEETA, Aveiro University, Aveiro, Portugal*
[*] *Corresponding author. E-mail: usama81818@nahrainuniv.edu.iq ; mohit.e15793@cumail.in*

Received: Dec. 10, 2025; Accepted: Mar. 31, 2026

The aim of the research is to compare the erosion performance under the effect of polyurethane coated and uncoated wind turbine blade (WTB) with Glass Fiber Reinforced Polymer (GFRP) material in offshore environmental conditions. The experiments were conducted on erosion tester using two parameters such as impact velocity (60, 90,120 m/s) and impact angle (30°,45°,60°). The experimental design was generated with the help Taguchi L9 array. Polyurethane spray coating was applied and offshore conditions were simulated using salt water. Furthermore, SEM (Scanning Electron Microscope) testing was done to study the surface morphology and Minitab software was used for statistic and Origin software was used to create graphs. The main finding shows that the impact velocity is the most influencing factor as compared to impact angle. Moreover, the surface morphology reveals the ductile mechanism of erosion and 93% more mass loss was measured in uncoated surface than coated surface.

Keywords: Taguchi; Erosion; Wind Turbine Blade; Composites; Scanning Electron Microscope; Polyurethane Coating.

http://dx.doi.org/10.6180/jase.202609_32.019

1. Introduction

The electricity production using renewable sources is in demand since ages and wind power mills are one of those resources. The fossil fuels are limited and when burnt pollute environment on the other hand renewable sources provide clean and cost-effective energy without harming the environment [1]. The increasing importance of the wind turbines in electricity generation also attracted the interest of researchers in the challenges faced in this field, especially blade degradation due to water drop erosion [2]. The erosion mass loss from the surface due to rubbing action and in case of WTB erosion insects, raindrops, hailstorms, and ultraviolet rays are main reasons of erosion [3]. The erosion increases the surface roughness which increase the drag and reduce lift, as a result, annual energy production (AEP) decreases [4]. Moreover, eroded if not controlled can lead to reduce in life of blade and sometimes also severe accident can occur [5, 6]. The rain drops falls from different height and strike the blade surface at different velocity and angle

[7]. The repeated impact of drops on the surface form pits and further increase the size which can increase the drag value by $6-500\%$ [8]. Some scholars have already found the relation between drag and AEP and they revealed that 80% increase in drag can drop 5% and 400-500% drag can reduce 25% AEP [9–11]. Various factors such as impact velocity, impact angle, size of raindrops, surface conditions and environmental conditions influence the erosion [12, 13]. The impact velocity and angle are important factors to study because when drops with same velocity strikes at different angles shows unique performance and their combined relation can be helpful to design the blades[14, 15]. Moreover, relation between surface roughness and impact velocity is exponential and it can increase the surface roughness up to three times in severe conditions [16, 17]. It produces a hammering force when hit by the surface, which causes material erosion and this force is directly related to velocity [18, 19]. This is also discovered by some scholars that drop size also affect the erosion such a study was conducted using $0.76\ \text{mm}-3.5\ \text{mm}$ diameters drops and $90\ \text{m/s}-150\ \text{m/s}$ velocity, its results shows that smaller drops are less harmful for blades as compared to larger size drops [20].

Another important parameter to study is impact angle which can be defined as angle between falling drop and blade surface [21]. Due to various blade portions experience varied angles due to curvature and rotation, the impact angle is crucial in wind turbine blade erosion [22]. It controls the primary damage process, which includes normal hammering stresses at perpendicular strikes and shear-induced cutting at oblique impacts. For coating optimization and the reduction of aerodynamic losses that lower Annual Energy Production (AEP), a precise understanding of this parameter is essential [23]. The blade surface becomes rougher and pits are created as raindrops hit it. Some scholars investigated different impact angles ranging from 45° to 90° at a constant velocity of $20\ \text{m/s}$ and found that the maximum erosion occurred at a negative impact angle of 45° [24]. Moreover, offshore environmental conditions are severe as compared to onshore conditions. Offshore conditions have saline environment, more material loss and hence high maintenance required [25, 26].

The literature review indicates that while some study has been done on WTB erosion, the processes of erosion, the effects of different factors, and the performance of various coatings remain unclear. The effects of two parameters impact angle and impact velocity on WTB erosion were examined in this work using a Taguchi experimental strategy. Experiments were performed using a Wind Turbine Blade Erosion Tester (WTBET) on both coated and uncoated surfaces to systematically evaluate their erosion behavior. Flow Chart of real-world application of study has been depicted in Fig. 1.

2. Materials and methods

A wind turbine blade erosion tester was used to conduct the experiments shown in Fig. 2. The different components were employed for various purposes, such as a water drum for storing water, an electric motor for rotating the whirling arms at different speeds, and sample holders for securing the specimens at the required testing angles. Supporting arms were used to hold the metallic wire ring, in which holes were created to fix the needles for producing 3 mm-sized drops. In addition, a pump was placed inside the drum to draw water and deliver it to the needles fixed in the metallic ring.

Fig. 3. presents the GFRP material samples with dimensions of 50 mm (length) $\times$25 mm (width) $\times$3 mm (thickness) employed in the experimental investigations. The primary reason for the widespread use of GFRP material in the production of WTB is its exceptional erosion resistance, lightweight design, corrosion resistance, and fatigue resistance. Polyurethane coating was applied to the surface due to its excellent abrasion and wear resistance [27]. To evaluate its performance, a coating thickness of $400-500\mu$ m was employed, as illustrated in the cross-sectional SEM image shown inFig. 4.Fig. 5 depicts the flowchart of proposed work.

Table 1 summarizes the key mechanical and adhesion properties of the two-component (2 K) polyurethane coating used in this study. The reported values were obtained from manufacturer datasheets and standardized test methods. These properties are characteristic of elastomeric polyurethane coatings typically used to protect GFRP members from erosion. GM GFRP substrates were also mechanically sanded with fine abrasive paper to enhance the degree of surface roughness prior to coating application and cleaned with solvents to remove impurities. A polyurethane compatible primer was employed for adhesion promotion. A two-component polyurethane coating was then applied and cured under ambient laboratory conditions (room temperature and moderate relative humidity). The coated specimens were allowed to cure for 24 hours to ensure complete cross-linking before erosion testing.

2.1. Data Processing

Table 2 presents the parameters used in the experiments and their corresponding levels. The impact velocity depends on wind speed, blade rotation, and drop trajectory.

Table 1. Properties of PU Coating Samples

Property	Symbol	Value	Test Method / Source
Hardness	Shore A	80-90	ASTM D2240 (manufacturer datasheet)
Elastic modulus	E (MPa)	15 – 30MPa	ASTM D412 (datasheet)
Tensile strength	σt (MPa)	20 – –35 MPa	ASTM D412 (datasheet)
Elongation at break	ε (%)	300-600 %	ASTM D412 (datasheet)
Adhesion strength to GFRP	MPa	5 – 8MPa	ASTM D4541 (pulloff test / datasheet)
Coating type	-	2 K polyurethane (elastomeric)	-

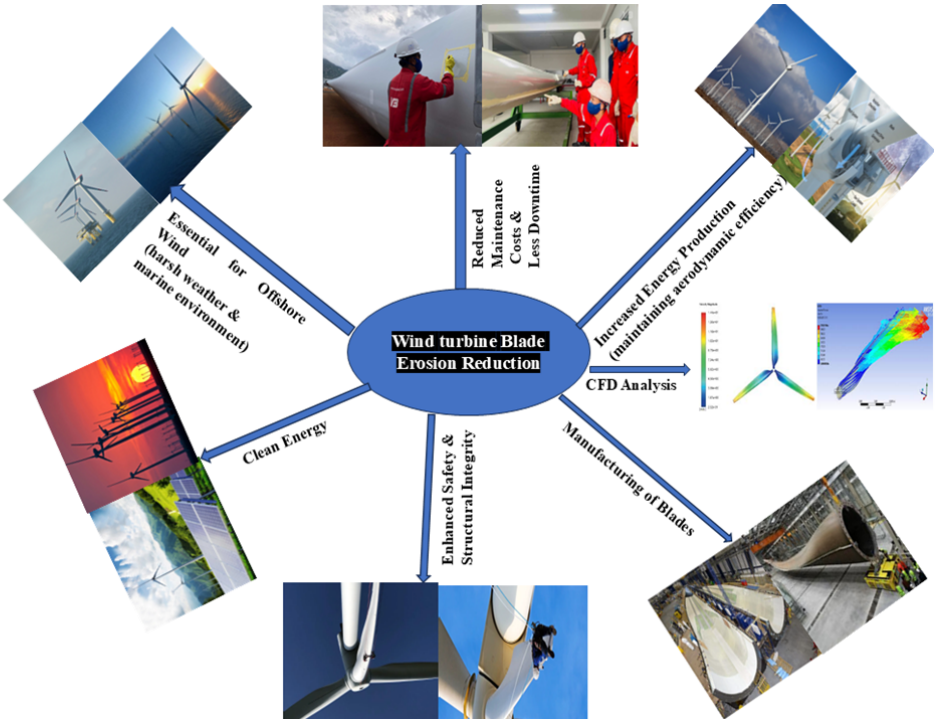

Fig. 1. Real-world application of the proposed work

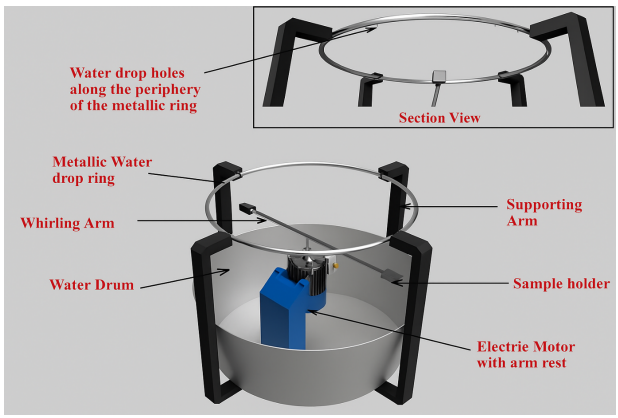

Fig. 2. Wind Turbine Blade Erosion Tester

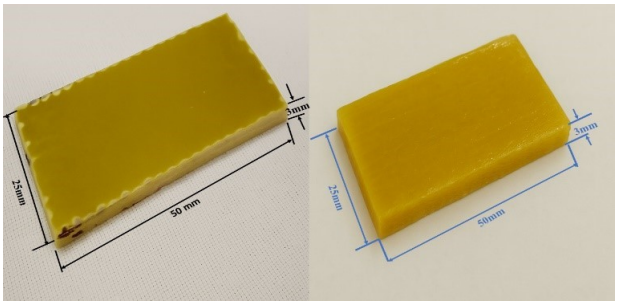

Fig. 3. (a) Uncoated (b) Coated

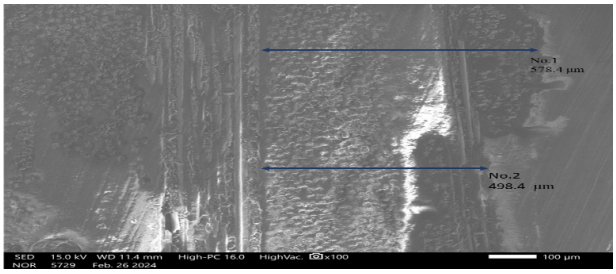

Fig. 4. Cross SEM of Polyurethane Coating

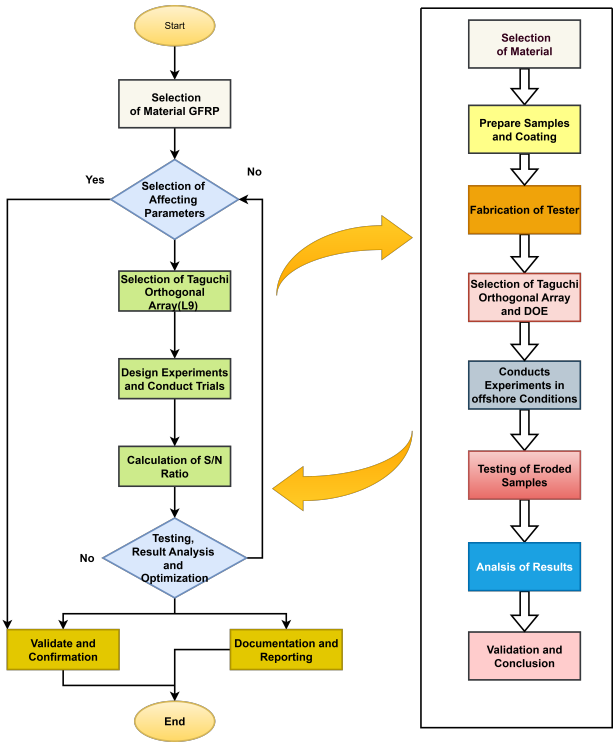

Fig. 5. Flowchart of Proposed Work

Here is how it is typically calculated:

2.1.1. Tangential Velocity of the Blade (U_t)

At a given radial position r on the blade:

$$U_t = \omega.r. \tag{1}$$

Where:
ω = angular velocity of the rotor (rad/s) $= 2\pi$RPM/60
r = radial distance from hub center to point of interest (m).

2.1.2. Relative Wind Velocity (U_{rel})

The wind speed (U∞) combines with the tangential blade speed to give the relative velocity:

$$U_{rel} = \sqrt{(U_\infty^2 + U_t^2)} \tag{2}$$

This is the velocity at which rain/particles approach the blade section.

2.1.3. Impact Velocity of Raindrop (V_{imp})

The raindrop does not always strike perpendicular. Considering the angle of attack (θ) of the drop trajectory relative to the blade:

$$V_{imp} = U_{rel} \cdot \cos(\theta). \tag{3}$$

In rain erosion test rigs the impact angle can be set mechanically by tilting the specimen using protractor. Here, the impact angle is not "measured" but controlled (such as $30°, 45°, 60°$).

Drop diameter and run time were assumed constant i.e. 3 mm and 120 minutes respectively. Raindrops were used as the erodent, and to simulate offshore environmental conditions, a 3% NaCl solution was used. All experiments were conducted at ambient laboratory temperature ($\sim 25°$C), and the solution pH remained approximately neutral. Electrical conduction was based on the constant salinity, and no evaporation effect appeared during the tests. These constants were held constant for all the test cases to facilitate the association between different acts. In the current study, impact velocity ($60 - 120$ m/s), impact angle ($30° - 60°$) and surface conditions (coated and uncoated polyurethane-based coating) are chosen as main factors, because they were identified to be most important factors affecting rain erosion under offshore operating condition. The droplet size (3 mm) was chosen to represent heavy rain that is typically reported in erosion studies, and the exposure time was set at 120 min which would simulate sustained offshore rainfall. By setting these parameters, fixing the tests with welldefined conditions and understanding the dominant erosion mechanisms could be performed.

Table 2. Ranges of taken factors in the proposed work.

Impact Velocity	60 m/s − 120 m/s
Impact Angle	30° − 60°
Surface Conditions	Polyurethane Based Coated and Uncoated
Drop Diameter	3 mm
Samples Size	50 mm × 25 mm × 3 mm
Environmental Conditions	Offshore
Run Time per Experiment	120 minutes

3. Result and discussion

In the design of experiments, two parameters were varied at three levels each, and a robust DOE was developed using the Taguchi method. The Taguchi method is a type of systematic design of experiments (DOE) which enables the analysis for multiple control factors to be undertaken on system's performance but with fewer number of trials. In the current study, two control factors at three levels were considered, and an L9 orthogonal array was chosen based on Taguchi design for balanced and uncorrelated evaluation of these parameters. The orthogonal array works for the reduction of experimental effort to a sufficiently high statistical reliability. Signal-to-noise (S/N) ratio, which considers both average response and distribution were used to indicate system performance. The optimal S/N cut was chosen according to the goal of the analysis. The effects of each parameter were investigated by means of Main effect plots and the percent contributions of them were determined by carrying out Analysis of variance (ANOVA). The parameter contribution with maximum value was found to be the significant and optimum level of selected factors were confirmed through confirmation experiments. An L9 orthogonal array was employed, which required a total of nine experiments to identify the optimal combination of the two parameters and their levels. Each experimental condition was conducted in four replicates (n = 4) under identical test parameters. The reported results correspond to mean values, with measurement uncertainty and dispersion quantified using the standard deviation. Furthermore, the Taguchi technique has number advantages over other methods such as Reduced number of experiments, Systematic and structured approach, Identification of significant factors, Clear evaluation of factor interactions, Ease of interpretation (signal-to-noise ratio), and Integration with other improvement tools [28–30].

The experimental design and results are presented in Table 3.

3.1. Analysis of Experimental Results

In Table 3, mass loss was determined by weighing each sample before the experiments and subtracting the weight recorded after the experiments. The resulting mass loss values were then converted into signal-to-noise (S/N) ratios ('smaller-is-better') using Minitab software. The smaller is better type is used because smaller erosion is expected in all the experiments. In this case higher S/N means better design and less erosion and vice versa [31, 32].

$$\frac{S}{N} = -10 \log \left[\frac{1}{n} \sum_{i=1}^{n} E_i^2 \right] \tag{4}$$

In which n denotes number of experiments and E_i is erosion in i_{th} experiment.

A Taguchi signal-to-noise (S/N) ratio analysis is used to measure the sensitivity of parameters as it considers both the mean response value and its variation. The response tables show that impact velocity has the highest delta value and is the most significant factor to determine erosion severity. This is in agreement with erosion mechanics theory that indicates that erosion damage scales significantly with the kinetic energy of impinging droplets. The less negative delta for impact angle and surface condition imply a secondary, but still meaningful contribution. The best set of parameters found by the Taguchi is characterized by lower impact velocities, optimal impingement angle, and polyurethane adding over aluminium substrates, resulting in minimum erosion rate and dispersion.

From a practical perspective, these findings suggest that erosion mitigation strategies for wind turbine blades should prioritize leading-edge protection systems capable of withstanding high local tip velocities. The identified optimal parameter levels can guide the selection and placement of protective coatings, inform maintenance scheduling in high-rainfall regions, and support blade design optimization by targeting erosion-resistant materials in critical blade regions.

From Table 3, it is evident that the signal-to-noise ratio is higher for the coated samples, indicating less erosion compared to the uncoated surfaces. This result was anticipated, as the polyurethane coating provides erosion resistance, which has been confirmed experimentally. Moreover, the highest mass loss was observed at a velocity of 120 m/s and an impact angle of 45°, for both surface conditions

Table 3. Experimental Design with Results

S. No.	Parameters		Mass Loss (Grams)		S/N Ratio	
	Impact Velocity (m/s)	Impact Angle (Degree)	Uncoated	Coated	Uncoated	Coated
1	60	30	0.015	0.0010	36.4782	60.0000
2	60	45	0.023	0.0013	32.7654	57.7211
3	60	60	0.016	0.0011	35.9176	59.1721
4	90	30	0.018	0.0015	34.8945	56.4782
5	90	45	0.027	0.0019	31.3727	54.4249
6	90	60	0.023	0.0015	32.7654	56.4782
7	120	30	0.029	0.0020	30.7520	53.9794
8	120	45	0.035	0.0024	29.1186	52.3958
9	120	60	0.034	0.0024	29.3704	52.3958

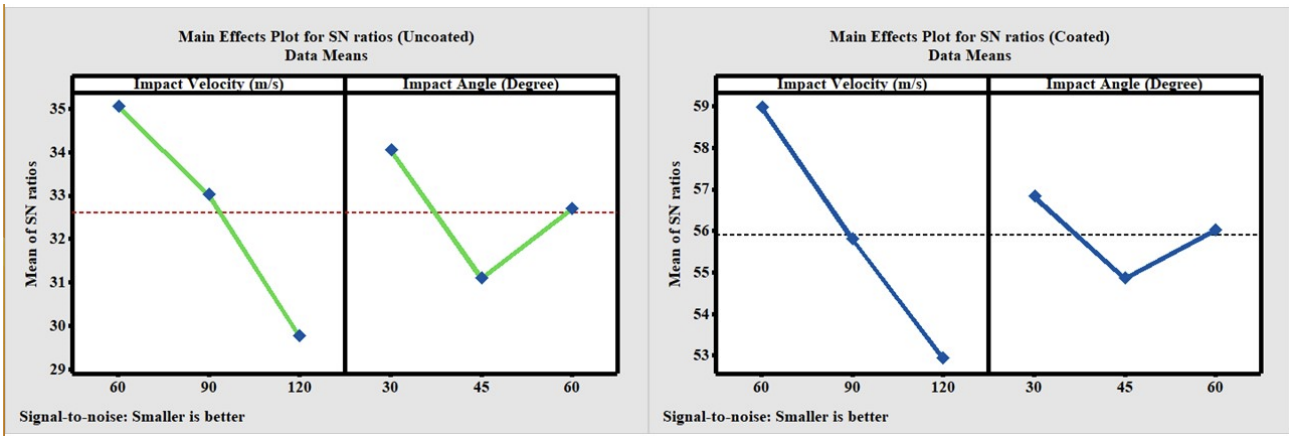

Fig. 6. Main effects plot for SN ratio (a) Uncoated (b) Coated

and the recorded maximum mass loss was 0.035 g for the uncoated surface and 0.0024 g for the coated surface. From the Table 4, only a marginal difference is observed at a velocity of 120 m/s and angles of 45° and 60°, indicating the dominance of the velocity factor, as at higher velocities the impact of angle becomes negligible [33].

3.2. Impact of Velocity and Angle

Table 4 presents the mean S/N ratio of impact velocity and impact angle at each level and shows the ranking of influencing factors based on the delta value. The delta is calculated by subtracting the lowest S/N value from the highest one. For both coated and uncoated samples, impact velocity is ranked first, indicating that it is a more influential factor than the impact angle [34, 35]. Moreover, according to the Taguchi method, a smaller S/N value corresponds to lower erosion resistance, and vice versa. As illustrated in Fig. 6, the S/N value reaches its minimum at higher impact velocities and at angles exceeding 30°, indicating that erosion is most severe under these conditions. The mean S/N ratio for the uncoated sample is 32.60 , whereas for the coated sample it is 55.90 and the mean line is represented with dotted line in Fig. 6. These outcomes indicate the erosion performance of samples is significantly influenced by both parameters; however, velocity is the more susceptible parameter. Impact was graded 1 based on the value of delta in Table 5, confirming that velocity is a significant factor that negatively impacts erosion. Furthermore, Fig. 7 shows that the greatest mass loss occurred at a velocity of 120 m/s and an angle of 45°, however the least mass loss recorded at 60 m/s and an angle of 30°.

3.3. Impact of Polyurethane Coating

In Fig. 8 it is evident that mass loss on uncoated is more than coated surfaces at all levels of impact velocity which is confirming the performance of polyurethane-based coating. The coating's strong erosion resistance quality provided protection for the coated samples [36]. The maximum mass loss of coating occurs at 120 m/s velocity (0.0022 grams) and 45°, impact angle (0.0018 grams), according to the mean mass loss Table 5 and Fig. 7. The impact velocity is the most important parameter that was chosen, and its maximum level of 120 m/s could erode only 0.0022 grams, demonstrating the coating's efficiency. By absorbing the kinetic energy of drops and forming a layer between the base material and the striking droplets, the polyurethane coat-

Table 4. Uncoated/ Coated Response Table for Signal to Noise Ratios means (Smaller is better)

Level	Uncoated		Coated	
	Impact Velocity (m/s)	Impact Angle (Degree)	Impact Velocity (m/s)	Impact Angle (Degree)
1	60	30	0.015	0.0010
2	60	45	0.023	0.0013
3	60	60	0.016	0.0011
Delta	90	30	0.018	0.0015
Rank	90	45	0.027	0.0019

Table 5. Uncoated/Coated Response Table for Means (mass loss)

Level	Uncoated		Coated	
	Impact Velocity (m/s)	Impact Angle (Degree)	Impact Velocity (m/s)	Impact Angle (Degree)
1	0.01800	0.02067	0.001133	0.001500
2	0.02267	0.02833	0.001633	0.001867
3	0.03267	0.02433	0.002267	0.001667
Delta	0.01467	0.00767	0.001133	0.000367
Rank	1	2	1	2

ing safeguards the substrate [37]. Fig. 9 compares the mass loss of coated and uncoated specimens at various impact angles. The erosion mechanism is ductile, as evidenced by the greatest mass loss seen at an angle of 45°.

When mass loss in coated and uncoated samples was examined across all trials, it was found that the uncoated samples had 93% greater mass loss. The flexibility, durability, and capacity of the polyurethane-based material to absorb the hammering pressure produced by drops made it extremely effective [38].

ANOVA was performed for both uncoated and polyurethane-coated GFRP specimens, and the results are included in the Table 6 and Table 7 respectively. For uncoated GFRP, impact velocity was found to be the dominant parameter, contributing 77.23% of the total variance ($F = 60.64$, $p = 0.001$), while impact angle showed a statistically significant but secondary contribution of 20.22%($F = 15.88, p = 0.013$). Similarly, for polyurethane-coated specimens, impact velocity remained the primary governing factor, accounting for 88.16% of the variance ($F = 67.00, p = 0.001$), whereas impact angle contributed 9.21%($F = 7.00, p = 0.049$). In both cases, the residual error was below 3%, indicating good experimental repeatability. Furthermore, four experimental replicates ($n = 4$) were conducted for each test condition, and mean values with standard deviations are now reported. These additions significantly enhance the statistical robustness of the study and provide strong quantitative support for the conclusions.

3.4. Analysis of Morphology

Most of the mass loss was seen at 120 m/s velocity, so only the highest level of velocity and two angles, 45° and 60°, were chosen for SEM testing; their results are shown in Figure **10**. In Fig. 10(a), ploughing and crater evidence are visible in testing, indicating very minimal degradation. Furthermore, the grooves in Fig. 10(b) are clearly visible; however, the coating remains undamaged since the fiber or substrate material is not exposed, even though some areas were impacted by debris. This analysis in Fig. 10(a) and (b) represents the performance of a coating with minimum damage because polyurethane acts as a protection [39, 40].

velocity (c) Uncoated 45° angle 120 m/s velocity (d) Uncoated 60° angle 120 m/s velocity Fig. 10(c) clearly displays a significantly damaged surface, exposed fibers, fractured fibers, and some debris. The explanation for this terrible damage could be the uncoated surface, the highest velocity, and the 45-degree impact angle, which cuts the most material because of micro-cutting. Another possible explanation is that cracks existed previously [41]. Figure 10(d) shows grooves, craters, and micro-cutting. All these features, including micro cutting, ploughing, grooves, and craters, illustrate the ductile erosion mechanism. The SEM research demonstrates that polyurethane coating is beneficial, however surface degradation increases dramatically without coating. Furthermore, the coating fills existent cracks and prevents them from escalating, increasing the life of the WTB even in adverse weather conditions [42].

Quantitative analysis of the eroded surfaces was performed to support the SEM observations Table 8. The results show that erosion pit depth increases markedly with

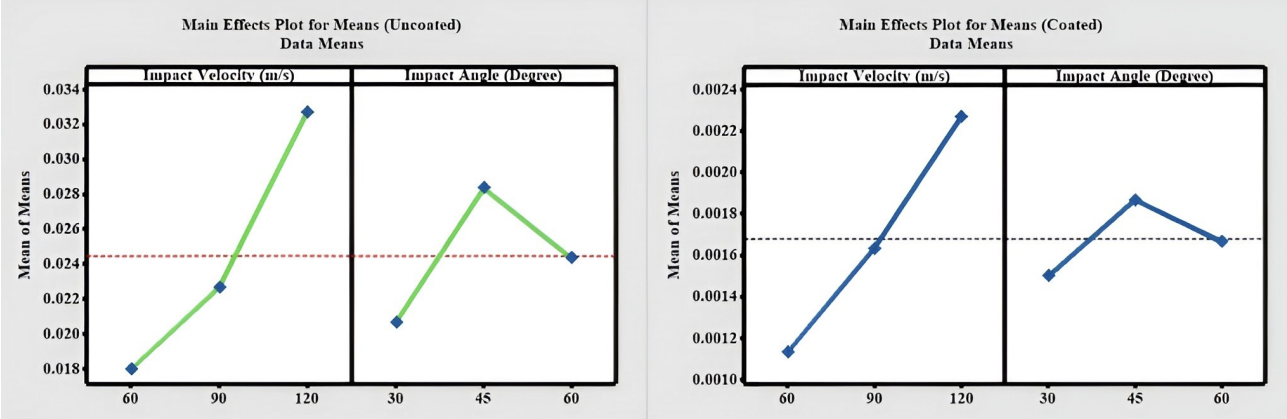

Fig. 7. Main effects plot for Means (a) Uncoated (b) Coated

Table 6. Analysis of Variance Uncoated

Level	Uncoated		Coated			
Source	DF	Seq SS	Contribution	Adj SS	Adj MS	F-Value	P-Value
Impact Angle (Degree)	2	0.000088	20.22%	0.000088	0.000044	15.88	0.013
Impact Velocity (m/s)	2	0.000337	77.23%	0.000337	0.000168	60.64	0.001
Error	4	0.000011	2.55%	0.000011	0.000003		
Total	8	0.000436	100.00%				

Table 7. Analysis of Variance Coated

Source	DF	Seq SS	Contribution	Adj SS	Adj MS	F-Value	P-Value
Impact Velocity (m/s)	2	0.000002	88.16%	0.000002	0.000001	67.00	0.001
Impact Angle (Degree)	2	0.000000	9.21%	0.000000	0.000000	7.00	0.049
Error	4	0.000000	2.63%	0.000000	0.000000		
Total	8	0.000002	100.00%				

Table 8. Quantitative SEM-Based Erosion Indicators for Coated and Uncoated GFRP

Condition	Velocity(m/s)	Angle ($^\circ$)	Erosion pit depth (μm)	Crack density (mm^{-2})	Surface roughness Ra (μm)
Uncoated GFRP	60	30	6.2 ± 0.8	12 ± 2	1.45 ± 0.12
Uncoated GFRP	90	45	11.8 ± 1.3	24 ± 3	2.76 ± 0.18
Uncoated GFRP	120	60	18.6 ± 1.9	39 ± 4	4.12 ± 0.25
PU-coated GFRP	60	30	2.1 ± 0.4	4 ± 1	0.62 ± 0.08
PU-coated GFRP	90	45	4.7 ± 0.6	9 ± 2	1.14 ± 0.10
PU-coated GFRP	120	60	7.9 ± 0.9	16 ± 2	1.98 ± 0.15

impact velocity, rising from approximately 6μ m at 60 m/s to nearly 19μ m at 120 m/s for uncoated GFRP, confirming the dominant role of droplet kinetic energy in erosion damage. A corresponding increase in surface roughness and crack density was observed, indicating progressive matrix degradation and subsurface damage accumulation at higher velocities. Impact angle exerted a secondary influence, primarily affecting crack density, crack orientation, and surface morphology rather than pit depth, as higher angles promote increased normal stress leading to localized matrix fatigue and partial fiber exposure. In contrast, polyurethane-coated specimens exhibited significantly lower erosion pit depths, reduced crack density, and smoother post-erosion surfaces across all test conditions. Even at the highest impact velocity, the pit depth of coated samples remained below 8μ m, demonstrating the coating's effectiveness in dissipating impact energy and delaying damage initiation. Overall, these quantitative indicators provide direct microstructural evidence supporting the macroscopic erosion trends and confirm that impact velocity is the dominant governing parameter, while the polyurethane coating substantially mitigates erosion sever-

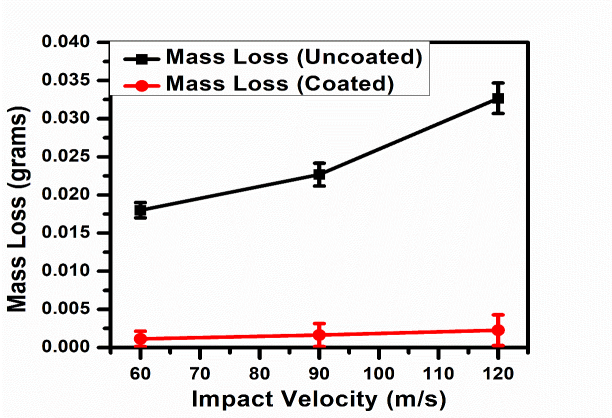

Fig. 8. Mass Loss Due to Impact Velocity

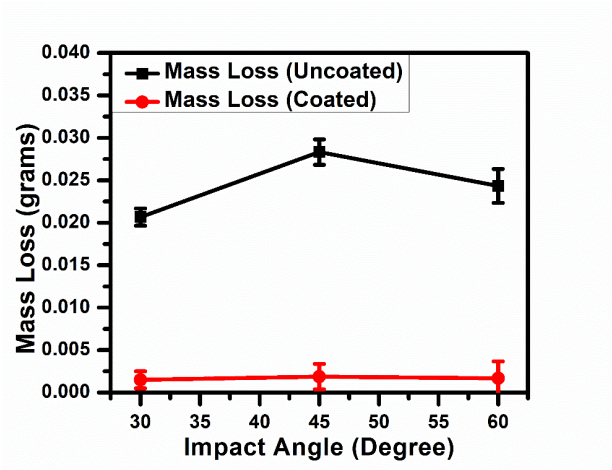

Fig. 9. Mass Loss Due to Impact Angle Comparison

ity under offshore-relevant conditions.

While the present experiments were conducted on flat coupon specimens to ensure controlled and repeatable conditions, it is recognized that erosion of full-scale wind turbine blades is influenced by additional factors such as blade curvature, radial velocity gradients, aerodynamic interaction between air and rain droplets, turbulence, oblique rainfall, and non-uniform rain flux. The chosen ranges of velocity and impact angle represent local working conditions at blade leading edges, especially in the outer span. In the future, aerodynamic coupling and blade level geometries will be included in the present method.

According to the results of experiments, impact velocity is the most significant parameter affecting rain-induced erosion and then followed by impact angle. The origin of this phenomenon is the strong influence on erosion damage of droplet kinetic energy, which depends quadratically on impact velocity. With the increase of impact velocity, the amplitude of generated stress waves at the liquid-solid interface is significantly increased, thus resulting in enhancement of localized deformation, micro-cracking and material removal. In contrast, the impact angle has an effect mainly in terms of normal and tangential momentum distributions. At shallower slanted angles, higher tangential components should contribute to droplet spreading and sliding that lowered the effective normal stress on the surface. With the increment of the impact angle normal component plays a more important role and thus increases localized stress, but it is still weaker than velocity-dependent energy amplification. This is why the effects of impact angle differences have secondary effects compared to impact velocity's governing role. The trends seen are in accordance with erosion mechanicals and rain erosion theories, extant in literature, where velocity is known to be the chief inducer of severity erosive for polymeric (and elastomeric) coatings. The dominance of impact velocity observed herein matches findings from previous studies into rain-induced erosion of polymer composites (18) and wind turbine blade materials, in which the severity of erosion has been found to scale significantly with the kinetic energy of droplets. Other researches on GFRP and polyurethane based leading edge protection systems also report velocity to be the dominant parameter, particularly at increasing relative tip speeds. The current finding substantiates these observations under offshore-based saline conditions and extended periods of exposure. With regard to impact angle, a secondary, but nonetheless significant effect has been reported by previous works due to normal and tangential differences in droplet momentum. The trends seen here are consistent with those earlier findings and further serve to elucidate how energy dissipation and surface compliance mediated by elastomeric polyurethane coatings modulate angle sensitivity. In contrast to previous coupon-scale studies under dry and non-saline exposure, the present study builds upon current understanding by including offshore environmental simulation and direct comparison of coated and uncoated GFRP surfaces. This leads to a more realistic evaluation of rain erosion behaviour for wind turbine blade leading edges in offshore conditions.

4. Conclusion

In the current proposed work, the performance of a rain eroded polyurethane coating was studied under oceanic rain erosion conditions with variations in impact velocity and impact angle. The findings indicate that the polyurethane coating provides good protection to GFRP surface as the boundary and receiver of buffering repeatedly hammering pressure from raindrop impact. It also fills in surface defects and inhibits crack initiation and propaga-

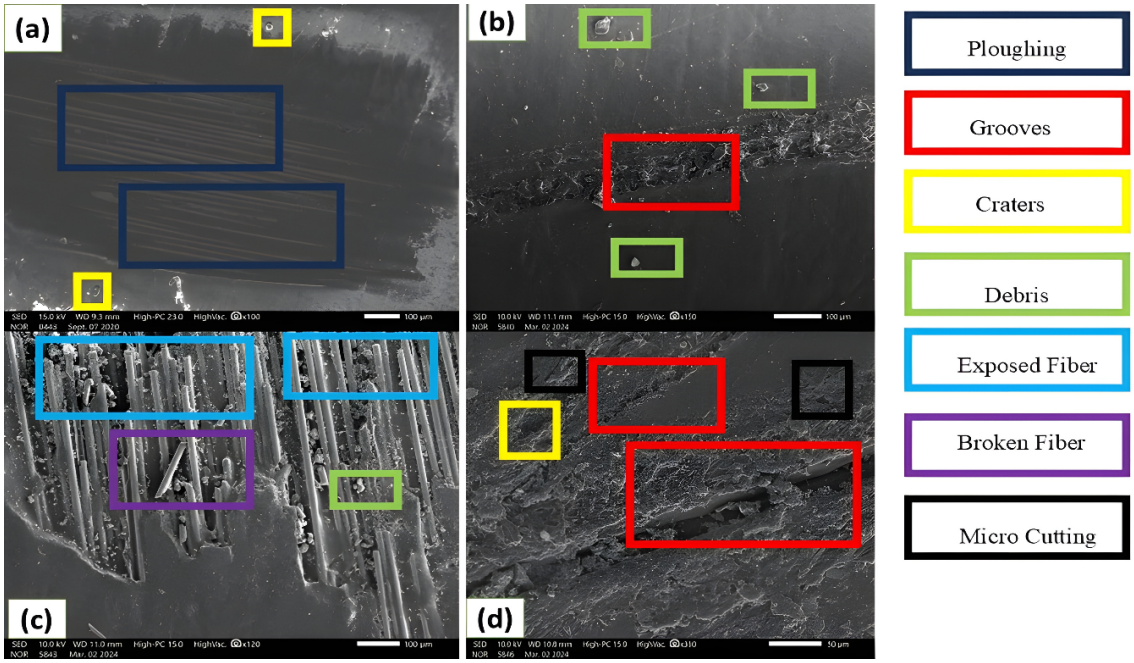

Fig. 10. SEM Analysis (a) Coated 60° angle 120 m/s velocity (b) Coated 45° angle 120 m/s

tion, resulting in a 93%-mass loss reduction compared to uncoated GFRP. Maximum erosion was experienced at 45° angle of impact and a velocity of 120 m/s indicating the complex effect of normal as well as tangential stresses. SEM observations revealed mainly the ductile type of erosion. The results clarify the dominant importance of impact at higher velocity in erosion damage, and stresses the role of polyurethane coatings in prolonging service life of blades. Such results could be utilized for reference in choosing the coating, estimating the blade life and planning the wind power maintenance on offshore wind turbine. Scaling effects and aerodynamic interactions were not taken into account, but should be addressed in future research.

References

[1] T. H. Malik and C. Bak, (2025) *"Challenges in Detecting Wind Turbine Power Loss: The Effects of Blade Erosion, Turbulence, and Time Averaging"* **Wind Energy Science *10***(1): 227–243. DOI: 10.5194/wes-10-227-2025.

[2] P. Rao and L. Mulky, (2023) *"Erosion-Corrosion of Materials in Industrial Equipment: A Review"* **ChemElectroChem *10***(16): e202300152. DOI: 10.1002/celc.202300152.

[3] F. Papi, F. Balduzzi, G. Ferrara, and A. Bianchini, (2021) *"Uncertainty Quantification on the Effects of Rain-Induced Erosion on Annual Energy Production and Performance of a Multi-MW Wind Turbine"* **Renewable Energy *165***: 701–715. DOI: 10.1016/j.renene.2020.11.071.

[4] J. Zhou, B. Han, and H. Wang, (2025) *"Surface Roughness Characteristics and Their Influence on Wind Erosion and Sand Movement"* **Atmosphere *16***(4): 443. DOI: 10.3390/atmos16040443.

[5] W. Han, J. Kim, and B. Kim, (2018) *"Effects of Contamination and Erosion at the Leading Edge of Blade Tip Airfoils on the Annual Energy Production of Wind Turbines"* **Renewable Energy *115***: 817–823. DOI: 10.1016/j.renene.2017.09.002.

[6] P. Yang, W. Yue, J. Li, G. Bin, and C. Li, (2022) *"Review of Damage Mechanism and Protection of Aero-Engine Blades Based on Impact Properties"* **Engineering Failure Analysis *140***: 106570. DOI: 10.1016/j.engfailanal.2022.106570.

[7] A. Castorrini, A. Ortolani, and M. S. Campobasso, (2023) *"Assessing the Progression of Wind Turbine Energy Yield Losses Due to Blade Erosion by Resolving Damage Geometries from Lab Tests and Field Observations"* **Renewable Energy *218***: 119256. DOI: 10.1016/j.renene.2023.119256.

[8] M. Carraro, F. De Vanna, F. Zweiri, E. Benini, A. Heidari, and H. Hadavinia, (2022) *"CFD Modeling of Wind Turbine Blades with Eroded Leading Edge"* **Fluids *7***(9): 302. DOI: 10.3390/fluids7090302.

[9] A. Singh, G. Singh, and S. Kumar, (2025) *"Comparative Analysis on Erosion Performance of Thin Coated GFRP Laminates in Offshore Conditions"* **Pigment &**

Resin Technology *54*(6): 820–828. DOI: 10.1108/PRT-07-2024-0071.

[10] M. S. Campobasso, A. Castorrini, L. Cappugi, and A. Bonfiglioli, (2022) *"Experimentally Validated Three-Dimensional Computational Aerodynamics of Wind Turbine Blade Sections Featuring Leading Edge Erosion Cavities"* **Wind Energy *25***(1): 168–189. DOI: 10.1002/we.2666.

[11] J. E. Zárate, M. D. L. G. López, J. A. C. Troyo, and L. Trujillo, (2022) *"Analysis and Detection of Erosion in Wind Turbine Blades"* **Mathematical and Computational Applications *27***(1): 5. DOI: 10 . 3390 / mca27010005.

[12] J. C. López, A. Kolios, L. Wang, and M. Chiachio, (2023) *"A Wind Turbine Blade Leading Edge Rain Erosion Computational Framework"* **Renewable Energy *203***: 131–141. DOI: 10.1016/j.renene.2022.12.050.

[13] N. A. W. A. Yusof, T. F. Algaddaime, and M. M. Stack, (2025) *"Advancements and Challenges in Coatings for Wind Turbine Blade Raindrop Erosion"* **Sustainability *17***(21): 9611. DOI: 10.3390/su17219611.

[14] L. Shi, H. Chen, S. Wang, L. Zhang, and X. Kou, (2025) *"Experimental Study on Static Ice Adhesion Characteristics of Wind Turbine Blade Surfaces After Sand Erosion"* **Coatings *15***(8): 955. DOI: 10.3390/coatings15080955.

[15] M. Sha, Y. Li, Y. Sun, Y. Liu, A. Mednikov, and A. Tkhabisimov, (2025) *"Experimental Study on Solid Particle Erosion of Protective Aircraft Coatings at Different Impact Angles"* **Reviews on Advanced Materials Science *64***(1): 20250100. DOI: 10.1515/rams-2025-0100.

[16] L. M. J. Mishnaevsky, A. Tempelis, N. Kuthe, and P. Mahajan, (2023) *"Recent Developments in the Protection of Wind Turbine Blades Against Leading Edge Erosion: Materials Solutions and Predictive Modelling"* **Renewable Energy *215***: 118966. DOI: 10.1016/j.renene.2023.118966.

[17] A. Tempelis and L. M. J. Mishnaevsky, (2025) *"Coating Material Loss and Surface Roughening Due to Leading Edge Erosion of Wind Turbine Blades: Probabilistic Analysis"* **Wear *566***: 205755. DOI: 10.1016/j.wear.2025.205755.

[18] A. Singh, G. Singh, and G. Singh, (2025) *"Comparative Erosion Wear Analysis of Polyurethane-Coated and Uncoated GFRP Wind Turbine Blades Under Onshore Conditions"* **Particulate Science and Technology**: 1–10. DOI: 10.1080/02726351.2025.2521324.

[19] Q. L. Oddo, Q. M. Ansari, F. Sánchez, L. M. J. Mishnaevsky, and T. M. Young, (2025) *"Stress Development in Droplet Impact Analysis of Rain Erosion Damage on Wind Turbine Blades"* **Applied Sciences *15***(15): 8682. DOI: 10.3390/app15158682.

[20] J. I. Bech, N. F. J. Johansen, M. B. Madsen, Á. Hannesdóttir, and C. B. Hasager, (2022) *"Experimental Study on the Effect of Drop Size in Rain Erosion Test and on Lifetime Prediction of Wind Turbine Blades"* **Renewable Energy *197***: 776–789. DOI: 10.1016/j.renene.2022.06.127.

[21] S. Groucott, K. Pugh, I. Zekos, and M. M. Stack, (2021) *"A Study of Raindrop Impacts on a Wind Turbine Material: Velocity and Impact Angle Effects on Erosion Maps at Various Exposure Times"* **Lubricants *9***(6): 60. DOI: 10.3390/lubricants9060060.

[22] M. Godfrey, O. Siederer, J. Zekonyte, I. Barbaros, and R. Wood, (2021) *"The Effect of Temperature on the Erosion of Polyurethane Coatings for Wind Turbine Leading Edge Protection"* **Wear *476***: 203720. DOI: 10.1016/j.wear.2021.203720.

[23] K. Vimalakanthan, H. van der Mijle Meijer, I. Bakhmet, and G. Schepers, (2023) *"Computational Fluid Dynamics Modeling of Actual Eroded Wind Turbine Blades"* **Wind Energy Science *8***(1): 41–69. DOI: 10.5194/wes-8-41-2023.

[24] K. Anderson, N. Azimy, and S. Karimi, (2025) *"Comparative Investigation Between Different Impact Angles for the Water Droplet Erosion of Wind Turbine Blades"* **Wear**: 205768. DOI: 10.1016/j.wear.2025.205768.

[25] A. S. Verma, Z. Jiang, Z. Ren, W. Hu, and J. J. Teuwen, (2021) *"Effects of Onshore and Offshore Environmental Parameters on the Leading Edge Erosion of Wind Turbine Blades"* **Journal of Offshore Mechanics and Arctic Engineering *143***(4): 042001. DOI: 10.1115/1.4049248.

[26] Z. Mu, W. Guo, Y. Li, and K. Tagawa, (2023) *"Wind Tunnel Test of Ice Accretion on Blade Airfoil for Wind Turbine under Offshore Atmospheric Condition"* **Renewable Energy *209***: 42–52. DOI: 10.1016/j.renene.2023.03.126.

[27] F. Ascione, G. Maselli, and A. Nesticò, (2024) *"Sustainable Materials Selection in Industrial Construction"* **Journal of Cleaner Production *475***: 143641. DOI: 10.1016/j.jclepro.2024.143641.

[28] A. V. U. K. Kandala, D. G. Solomon, and J. J. Arulraj, (2022) *"Advantages of Taguchi Method Compared to Response Surface Methodology for Achieving the Best Surface Finish in WEDM"* **Journal of Mechanical Engineering (JMechE) *19***(1): 185–200. URL: https://ir.uitm.edu.my/id/eprint/60593.

[29] M. W. Hisam, A. A. Dar, M. O. Elrasheed, M. S. Khan, R. Gera, and I. Azad, (2024) *"The Versatility of the Taguchi Method: Optimizing Experiments Across Diverse Disciplines"* **Journal of Statistical Theory and Applications** ***23***(4): 365–389. DOI: 10.1007/s44199-024-00093-9.

[30] J. Antony, S. Bhat, A. Mittal, R. Jayaraman, E. V. Gijo, and E. A. Cudney, (2024) *"Application of Taguchi Design of Experiments in the Food Industry"* **Total Quality Management & Business Excellence** ***35***(5–6): 687–712. DOI: 10.1080/14783363.2024.2331758.

[31] G. Box, (1988) *"Signal-to-Noise Ratios, Performance Criteria, and Transformations"* **Technometrics** ***30***(1): 1–17. DOI: 10.1080/00401706.1988.10488313.

[32] K. Kumar, S. Kumar, C. B. Tripathi, H. Sharma, and S. B. Prasad, (2020) *"Parametric Optimization of Slurry Erosion Behaviour of Brass"* **Materials Today: Proceedings** ***26***: 1604–1609. DOI: 10.1016/j.matpr.2020.02.330.

[33] R. Prieto and T. Karlsson, (2021) *"A Model to Estimate the Effect of Variables Causing Erosion in Wind Turbine Blades"* **Wind Energy** ***24***(9): 1031–1044. DOI: 10.1002/we.2615.

[34] W. Zhou, D. Zhang, and M. Yang, (2024) *"Effects of Surface Curvature on Rain Erosion of Wind Turbine Blades Under High-Velocity Impact"* **Heliyon** ***10***(23): DOI: 10.1016/j.heliyon.2024.e40761.

[35] K. Pugh, J. W. Nash, G. Reaburn, and M. M. Stack, (2021) *"On Analytical Tools for Assessing the Raindrop Erosion of Wind Turbine Blades"* **Renewable and Sustainable Energy Reviews** ***137***: 110611. DOI: 10.1016/j.rser.2020.110611.

[36] A. F. Alajmi and M. Ramulu, (2025) *"The Effectiveness of Graphene and Polyurethane Multilayer Coating on Minimizing the Leading-Edge Erosion of Wind Turbine Blades"* **Results in Engineering** ***26***: 104804. DOI: 10.1016/j.rineng.2025.104804.

[37] K. M. Jespersen, M. Eftekhar, N. F. J. Johansen, J. I. Bech, L. M. J. Mishnaevsky, and L. P. Mikkelsen, (2023) *"High Rate Response of Elastomeric Coatings for Wind Turbine Blade Erosion Protection"* **International Journal of Impact Engineering** ***179***: 104643. DOI: 10.1016/j.ijimpeng.2023.104643.

[38] Z. Zheng, H. Sun, W. Xue, D. Duan, G. Chen, X. Zhou, and J. Sun, (2024) *"Preparation of Protective Coatings for the Leading Edge of Wind Turbine Blades"* **Wear** ***558***: 205568. DOI: 10.1016/j.wear.2024.205568.

[39] H. Sun, Z. Zheng, W. Xue, J. Xu, F. Cao, D. Duan, and J. Sun, (2025) *"Preparation of Polyurethane Protective Coating with Different Pigment-to-Binder Ratios"* **Tribology International**: 110831. DOI: 10.1016/j.triboint.2025.110831.

[40] S. M. Pathak, V. P. Kumar, V. Bonu, L. M. J. Mishnaevsky, R. V. Lakshmi, P. Bera, and H. C. Barshilia, (2025) *"Enhancing Wind Turbine Blade Protection: Solid Particle Erosion Resistant Ceramic Oxides-Reinforced Epoxy Coatings"* **Renewable Energy** ***238***: 121681. DOI: 10.1016/j.renene.2024.121681.

[41] J. Bech and J. Simon, (2025) *"Fatigue crack growth in elastomers for leading edge erosion protection of wind turbine blades"* **Wind Energy Science Discussions** ***2025***: 1–32. DOI: https://doi.org/10.5194/wes-2025-247.

[42] E. Saenz, B. Mendez, and A. Munoz, (2022) *"Effect of Erosion Morphology on Wind Turbine Production Losses"* **Journal of Physics: Conference Series** ***2265***(3): 032059. DOI: 10.1088/1742-6596/2265/3/032059.